AUTHOR	Lucas Narciso, Tracy Ssali, Linshan Liu, Heather Biernaski, John Butler, Laura Morrison, Jennifer Hadway, Jeffrey Corsaut, Justin W Hicks, Michael C Langham, Felix W Wehrli, Hidehiro Iida and Keith St. Lawrence
TITLE	A Noninvasive Method for Quantifying Cerebral Metabolic Rate of Oxygen by Hybrid PET/MRI: Validation in a Porcine Model
YEAR	2021
DOI	10.2967/jnumed.120.260521
VERSION	Author's accepted manuscript
CITATION	Lucas Narciso, Tracy Ssali, Linshan Liu, Heather Biernaski, John Butler, Laura Morrison, Jennifer Hadway, Jeffrey Corsaut, Justin W Hicks, Michael C Langham, Felix W Wehrli, Hidehiro Iida and Keith St. Lawrence Journal of Nuclear Medicine March 2021, jnumed.120.260521; DOI: https://doi.org/10.2967/jnumed.120.260521

Validation of a non-invasive hybrid PET/MR method for imaging the cerebral metabolic rate of oxygen

Lucas Narciso[1,2], Tracy Ssali[1,2], Linshan Liu[1], Heather Biernaski[1], John Butler[1], Laura Morrison[1], Jennifer Hadway[1], Jeffrey Corsaut[1], Justin W. Hicks[1,2], Michael C. Langham[3], Felix W. Wehrli[3], Hidehiro Iida[4,5], Keith St Lawrence[1,2]

[1]*Lawson Health Research Institute, London, Ontario, Canada*

[2]*Department of Medical Biophysics, Western University, London, Ontario, Canada*

[3]*Department of Radiology, University of Pennsylvania Perelman School of Medicine, Philadelphia, USA*

[4]*University of Turku and Turku PET Centre, Turku, Finland*

[5]*Department of Radiology, National Cerebral Cardiovascular Center, Osaka, Japan*

Contact: Keith St Lawrence, Lawson Health Research Institute, 268 Grosvenor St., London, Ontario, N6A 4V2, Canada. E-mail: kstlaw@lawsonimaging.ca

Phone: +1-519-646-6100 x65737

Fax: +1-519-432-7367

ABSTRACT

The gold standard for imaging the cerebral metabolic rate of oxygen ($CMRO_2$) is with positron emission tomography (PET); however, it is an invasive and complex procedure that also requires correction for recirculating $[^{15}O]H_2O$ and the blood-borne activity. We propose a non-invasive reference-based hybrid PET/magnetic resonance imaging (MRI) method that uses functional MRI techniques to calibrate $[^{15}O]O_2$-PET data. Here, PET/MR imaging of oxidative metabolism (PMROx) was validated in an animal model by comparison to PET-alone measurements. Additionally, we investigated if the MRI-perfusion technique arterial spin labelling (ASL) could be used to further simplify PMROx by replacing $[^{15}O]H_2O$ PET, and if the PMROx was sensitive to anesthetics-induced changes in metabolism.

Methods: $[^{15}O]H_2O$ and $[^{15}O]O_2$ PET data were acquired in a hybrid PET/MR scanner (3 T Siemens Biograph mMR), together with simultaneous functional MRI (OxFlow and ASL), from juvenile pigs (n = 9). Animals were anesthetized with 3% isoflurane and 6 mL/kg/h propofol for the validation experiments and arterial sampling was performed for PET-alone measurements. PMROx estimates were obtained using whole-brain (WB) $CMRO_2$ from OxFlow and local CBF from either non-invasive $[^{15}O]H_2O$-PET or ASL ($PMROx_{ASL}$). Changes in metabolism were investigated by increasing the propofol infusion to 20 mL/kg/h.

Results: Good agreement and correlation were observed between regional $CMRO_2$ measurements from PMROx and PET-alone. No significant differences were found between OxFlow and PET-only measurements of WB oxygen extraction fraction (0.30 ± 0.09 and 0.31 ± 0.09) and CBF (54.1 ± 16.7 and 56.6 ± 21.0 mL/100g/min), or between PMROx and PET-only $CMRO_2$ estimates (1.89 ± 0.16 and 1.81 ± 0.10 mLO_2/100g/min). Moreover, PMROx and $PMROx_{ASL}$ were sensitive to propofol-induced reduction in $CMRO_2$.

Conclusion: This study provides initial validation of a non-invasive PET/MRI technique that circumvents many of the complexities of PET $CMRO_2$ imaging. PMROx does not require arterial sampling and has the potential to reduce PET imaging to $[^{15}O]O_2$ only; however, future validation involving human participants are required.

KEYWORDS

Cerebral blood flow, cerebral metabolic rate of oxygen, non-invasive PET, oxygen extraction fraction, PET/MRI

INTRODUCTION

Positron emission tomography (PET) imaging of cerebral oxidative metabolism was developed over thirty years ago and continues to prove a vital tool for understanding brain energetics and the role of altered metabolism in disease processes (*1*–*3*). PET remains the gold standard for imaging the cerebral metabolic rate of oxygen ($CMRO_2$); however, the original procedure is complex and long (*4*). In addition to radiolabelled oxygen, $[^{15}O]H_2O$ is needed to measure cerebral blood flow (CBF) and $[^{15}O]CO$ to measure the cerebral blood volume (CBV). Arterial blood sampling is required for each tracer, along with separating plasma and red blood cell activity for $[^{15}O]O_2$ to account for the increasing signal contribution from metabolically generated $[^{15}O]H_2O$ (recirculating water, RW). Efforts to reduce its complexity and duration have led to modelling approaches that eliminate the need for separate CBV imaging and estimating RW without separating blood samples (*5*,*6*). Alternately, the effects of RW can be minimized by short scan times following a single inhalation of $[^{15}O]O_2$ (*7*). More recently, approaches incorporating image-derived input functions have been proposed to avoid measuring the arterial input function (AIF), which is an invasive and inherently noisy procedure (*8*,*9*). However, the accuracy of these approaches depends on either an empirical factor relating the total AIF and its RW component, or careful measurement of a coefficient to scale the arterial time-activity curve (TAC).

We propose an alternative method to reduce the complexity, invasiveness, and duration of $CMRO_2$ imaging. Similar to Su *et al*. (*9*), this method takes advantage of simultaneous PET/MRI. However, rather than attempting to use MRI to help extract the AIF, the proposed hybrid approach incorporates complementary MRI techniques to measure whole-brain (WB) $CMRO_2$ to act as a reference region to calibrate dynamic $[^{15}O]$oxygen PET data. Analogous to a similar PET/MR technique for imaging CBF (*10*), this hybrid approach eliminates the need for arterial sampling.

Here, we implemented this reference-based approach, hereafter referred as PMROx (PET/MR imaging of oxidative metabolism), on a 3 T PET/MR scanner. The aim of this study is to validate PMROx in a large animal model by comparing to a previously validated dual-basis function method (DBFM) (*6*). In addition, we investigated if PMROx could be further simplified by incorporating CBF images from the MRI-based technique arterial spin labelling (ASL). This modification reduces PET imaging to only $[^{15}O]O_2$ and imaging duration to approximately 5 min since the MRI sequences can be run during the PET acquisition (*11*). In addition to validating PMROx, its sensitivity to changes in metabolism was investigated by altering the anesthetics administered to the animals.

MATERIALS AND METHODS

Animal experiments were conducted according to the regulations of the Canadian Council of Animal Care and approved by the Animal Care Committee at Western University. Prior to imaging, juvenile Duroc pigs were tracheotomized, and catheters inserted into the cephalic veins and femoral arteries. During imaging, the animals were mechanically ventilated and immobilized on a custom platform. Animals were anesthetized with 3% isoflurane and 6 mL/kg/h propofol during baseline. Each experiment began by collecting blood samples to measure the partial pressures of oxygen (P_aO_2) and carbon dioxide (P_aCO_2), plasma glucose concentration (*c*Glu), hematocrit, and hemoglobin concentration (Hb) using a blood gas analyzer. Throughout the experiment, end-tidal O_2 and CO_2, temperature, heart rate, and oxygen saturation were continuously monitored to ensure normal levels.

STUDY PROTOCOL

PET and MRI data were obtained on a 3 T Siemens Biograph mMR system using a 12-channel PET-compatible receiver head coil (Siemens GmbH). Each experiment was divided into two parts. First, the accuracy of PMROx was evaluated by measuring the AIFs of $[^{15}O]H_2O$ and $[^{15}O]O_2$, as required for the DBFM. Next, the sensitivity of PMROx to changes in cerebral metabolism was assessed by increasing the infusion rate of propofol to 20 mL/kg/h to induce a lower metabolic condition (LMC).

In both parts, PET imaging involved injecting $[^{15}O]H_2O$ to measure CBF, followed by inhalation of $[^{15}O]O_2$ to measure OEF. Concurrently, WB $CMRO_2$ was obtained by the MRI-sequence OxFlow (*12*), which combines phase-contrast MRI measurements of CBF from the internal carotid arteries (ICA) and basilar artery (BA), with venous oxygen saturation (S_vO_2)

measurements from the superior sagittal sinus (SSS) acquired with susceptibility-based oximetry (*13*). CBF images were collected using pseudo-continuous arterial spin labelling (pCASL). At the end of experiment, the animal was euthanized according to the animal care guidelines and transported to a CT scanner to obtain a post-mortem CT-based attenuation correction map (*17*).

PET IMAGING AND POSTPROCESSING

The PET protocol began with injecting [^{15}O]H_2O (460 ± 80 MBq; cephalic vein), followed by inhaling 2,200 MBq of [^{15}O]O_2. Both acquisitions involved 5 min of list-mode data acquisition. For DBFM, AIFs ($C_a^w(t)$ and $C_a^o(t)$) were determined by continuously withdrawing blood from a femoral artery and measuring the activity using an MR-compatible system (Swisstrace GmbH). The short tubing (15-cm length, 1.27-mm diameter) connecting the artery to the detector caused negligible dispersion at the withdrawal rate of 5 mL/min (*10*).

[^{15}O]H_2O and [^{15}O]O_2 were produced by (d,n) ^{14}N reaction in an onsite cyclotron (PETtrace 800, 16.5 MeV; GE Healthcare) (*14*). For [^{15}O]O_2 imaging, the radioactive gas was filtered prior to being transferred to the PET/MR suite via a stainless steel line (202-m long, 3-mm diameter). The line was connected to polyethylene tubing that directly fed into the inhalation tube of the animal (delivery rate of 1.5 L/min for 30 s). Expired gas was collected in a 200-L tank to hold it for seven half-lives (*15*).

Dynamic PET images were reconstructed into 48 time-frames (30×3s, 6×5s, 6×10s and 6×20s) using the e7-tools with a 3D-OSEM method (iterations/subsets, 4/21; matrix size, 344×344×127 voxels; field of view [FoV], 359×359×258 mm^3; voxel size, 1×1×2 mm^3; zoom factor, 2). Raw data were corrected for decay, random incidences, dead-time, detector normalization, data rebinning, and scatter. Absolute scatter correction was used for the [^{15}O]O_2

images, as recommended for 3D scanning (*16*). Reconstructed images were smoothed by a 4-mm Gaussian filter.

AIFs were decay corrected to the PET start-time, calibrated using pSample (PMOD 3.6), and denoised using a wavelet signal denoising function (MATLAB R2017b, Block James-Stein method). The $A_w(t)$ component of the measured [^{15}O]O_2 AIF was estimated using species-specific values after interpolating to the differences in weight (*18*).

MR IMAGING AND POSTPROCESSING

T_1-weighted images (Fig. 1A) were acquired using a magnetization-prepared rapid gradient-echo sequence (MPRAGE, repetition/echo/inversion times [TR/TE/TI], 2,000/2.98/900 ms; flip angle [α], 9º; FoV, 256×256 mm^2; 176 slices; isotropic voxel size, 1 mm^3), followed by time-of-flight images to identify the ICA and BA for phase-contrast imaging (Fig. 1B; TR/TE, 22/3.75 ms; α, 18º; FoV, 200×181 mm^2; 102 slices; voxel size, 0.3×0.3×1.5 mm^3; 40 mm saturation band) and the SSS for oximetry imaging (Fig. 1C; no saturation band).

The MRI sequences OxFlow and pCASL were acquired during PET acquisitions. The former alternates between the two slice locations to measure WB CBF and S_vO_2 (Fig. 1B-G; TR/TE/ΔTE, 35/7.025/2.5 ms; α, 25º; FoV, 208×208 mm^2; voxel size, 1.6×1.6×5.0 mm^3; velocity encoding [VENC], 60 cm/s; acquisition time, 1 min) (*12*). A 3-dimensional pCASL was implemented (TR/TE, 3,720/22.9 ms; FoV, 208×208 mm^2; 16 slices; voxel size, 3.3×3.3×5.0 mm^3; post-labelling delay/labelling duration, 1500/1800 ms; label plane offset, 60 mm; 16 measurements), alongside with proton density-weighted images with no labelling or background suppression pulses (M_0; TR, 7,000 ms).

OxFlow images were analyzed following the approach outlined by Jain *et al*. (*13*). Briefly, regions-of-interest (ROIs) were semi-automatically drawn in and surrounding the vessels on the magnitude image (Fig. 1D and F), then transferred to the phase image (Fig. 1E and G) to measure the mean phase difference ($\Delta\phi$) in the feeding arteries, and between the SSS and the surrounding tissue. The pCASL images were motion corrected, coregistered to M_0, and smoothed with a 4-mm Gaussian filter. CBF images were generated using the standard one-compartment model (*11*). For this analysis, the blood-brain partition coefficient of water was 0.90 mL/g, the longitudinal relaxation time of blood was 1.65 s, and the labelling efficiency was assumed to be 0.86. Images were coregistered to the PET space using SPM12 (https://www.fil.ion.ucl.ac.uk/spm/).

PET-ONLY CBF AND $CMRO_2$ IMAGING: DBFM

CBF (f_i) maps were generated from [^{15}O]H_2O PET by fitting the following equation to the TACs:

$$C_i(t) = f_i \cdot C_a^w(t) * e^{-k_{2i}t} + V_{b_i}^w \cdot C_a^w(t) \qquad (1)$$

where $C_i(t)$ is the local TAC, $C_a^w(t)$ the AIF, and the $*$ represents convolution. The fitting parameters were k_{2_i} (clearance constant rate), f_i, and $V_{b_i}^w$ (arterial blood volume). OEF (E_i) and $CMRO_2$ measurements were obtained by fitting [^{15}O]O_2 PET data to the equation (*6*):

$$C_i(t) = E_i \cdot f_i \cdot A_o(t) * e^{-k_{2i}t} + f_i \cdot A_w(t) * e^{-k_{2i}t} + V_{0_i}^o \cdot A_o(t) + V_{A_i}^w \cdot A_w(t) \qquad (2)$$

where $A_o(t)$ is the [^{15}O]O_2 component of the AIF. The fitting parameters were E_i, $V_{0_i}^o$ and $V_{A_i}^w$ ([^{15}O]O_2 and [^{15}O]H_2O blood volumes, respectively). All fitting was performed in MATLAB using the optimization routine *fmincon*. $CMRO_2$ was calculated by $CMRO_{2_i} = E_i \cdot f_i \cdot C_aO_2$, where

$C_aO_2 = 1.34 \cdot Hb \cdot S_aO_2 + 0.003 \cdot P_aO_2$, and S_aO_2 (arterial saturation of oxygen) was estimated using the P_aO_2 measurements (*19*).

PMROx

PMROx $CMRO_2$ images were generated from $^{15}O[O_2]$-PET data by (*20*):

$$CMRO_{2_i} = \boldsymbol{CMRO_{2_{wb}}} \left[\frac{\int_0^T C_i(t)dt + \frac{f_i}{p}\int_0^T \int_0^t C_i(s)ds\,dt}{\int_0^T C_{wb}(t)dt + \frac{\boldsymbol{f_{wb}}}{p}\int_0^T \int_0^t C_{wb}(s)ds\,dt} \right] \quad (3)$$

where $C(t)$ is the TAC, and T the scan time. The subscripts *i* and *wb* represent the i^{th} voxel and whole-brain, respectively. f_{wb} and $CMRO_{2_{wb}}$ were obtained from OxFlow, the latter by:

$$\boldsymbol{CMRO_{2_{wb}}} = C_aO_2 \cdot \boldsymbol{f_{wb}} \left(\frac{S_aO_2 - \boldsymbol{S_vO_2}}{S_aO_2} \right) \quad (4)$$

Local CBF was obtained using the non-invasive PET/MR approach described by Ssali *et al.* (*10*), in which WB CBF is used to calibrate $[^{15}O]H_2O$ PET data:

$$f_i = \frac{\int_0^T C_i(t)dt}{\frac{1}{\boldsymbol{f_{wb}}}\int_0^T C_{wb}(t)dt + \frac{1}{p}\left(\int_0^T \int_0^t C_{wb}(s)ds\,dt - \int_0^T \int_0^t C_i(s)ds\,dt\right)} \quad (5)$$

The feasibility of implementing pCASL into the PMROx approach was also evaluated. In this case, hereafter referred to as $PMROx_{ASL}$, f_i in Eq. (3)~~(3)~~ was obtained from the CBF images generated by pCASL.

REGIONAL CBF, OEF AND $CMRO_2$ MEASUREMENTS

ROIs were semi-automatically drawn on the MPRAGE images for each animal and then transferred to the corresponding CBF, OEF and $CMRO_2$ images. Measurements were acquired for cerebellum (4.2 ± 0.7 cm^3), diencephalon (4.7 ± 0.6 cm^3), and frontal (2.4 ± 0.6 cm^3), occipital (7.9 ± 1.5 cm^3), parietal (9.1 ± 1.6 cm^3) and temporal (6.0 ± 0.6 cm^3) lobes.

STATISTICS

Local measurements were compared using linear regression to obtain the Pearson correlation coefficient (ρ). Any potential bias was assessed using a one-sample *t*-test. Paired *t*-tests were performed to evaluate differences between measurements. Statistical significance was defined by $\alpha < 0.05$ and Bonferroni correction was performed when necessary. Measurements are expressed in terms of mean ± SD. Statistical tests were performed using SPSS (v26, https://www.ibm.com/analytics/spss-statistics-software).

RESULTS

Data from nine juvenile pigs were collected (age range 8-10 weeks; weight, 19 ± 2 kg; 5 female). In one experiment, only [^{15}O]H_2O data were acquired due to a technical issue with the [^{15}O]oxygen line. The LMC was successfully induced in six animals. Table 1 provides a summary of arterial blood measurements during baseline and LMC.

In three cases (one [^{15}O]H_2O and two [^{15}O]O_2), AIFs were not acquired due to clotting of the sampling line. In these cases, a population-based AIF was used. For the [^{15}O]H_2O case, the AIF was scaled by the injected dose (MBq). Since the administered activity was unknown for [^{15}O]O_2, the AIF was scaled to the mean jaw muscle activity (C_m) measured from a 50-mm^2 ROI. The appropriate scaling factor was determined by a combination of principal component and multiple linear regression analyses involving the measured AIFs.

VALIDATION

Average WB estimates of CBF, OEF and $CMRO_2$ from PET and PET/MR were in good agreement with no significant differences between techniques: 56.6 ± 21.0 mL/100g/min, 0.31 ± 0.09, and 1.81 ± 0.10 mLO_2/100g/min from DBFM and 54.1 ± 16.7 mL/100g/min, 0.30 ± 0.09 and 1.89 ± 0.16 mLO_2/100g/min from OxFlow/PMROx, respectively. Average WB-V_b^w from [^{15}O]H_2O-PET was 9.5 ± 4.0 mL/100g, and WB V_0^o and V_A^w values from [^{15}O]O_2-PET were 7.0 ± 1.0 mL/100g and 2.6 ± 6.7 mL/100g, respectively. WB V_A^w was small (< 2 mL/100g) for 7 of 8 animals; however, in one outlier it was 19.1 mL/100g.

Regional results of regression and correlation (Fig. 2) analyses from CBF, OEF and $CMRO_2$ measurements are summarized in Table 2. Significant correlations between regional CBF estimates from non-invasive PET/MR and DBFM were observed in all ROIs. The Bland-Altman

plot indicated a small, but significant, overestimation in local CBF measurements by non-invasive PET/MR. Strong correlations between regional OEF estimates from PMROx and DBFM were also observed (Fig. 2B and 3). Finally, regression between $CMRO_2$ estimates from the two techniques revealed good agreement with a moderate correlation and a small significant bias in the PMROx measurements.

PMROX$_{ASL}$

Average WB estimates of CBF and $CMRO_2$ from pCASL and PMROx$_{ASL}$ were 58.6 ± 20.4 mL/100g/min and 1.88 ± 0.24 mLO_2/100g/min, respectively, which were not significantly different from the PET-only results. Regional CBF, OEF and $CMRO_2$ measurements were successfully extracted from all ROIs (Table 2, Fig. 3 and 4), except for the cerebellum from one animal because this region was missing in the pCASL FoV. Strong regressions between DBFM and pCASL CBF estimates, and PMROx$_{ASL}$ OEF estimates, were observed. $CMRO_2$ values from PMROx$_{ASL}$ showed a moderate correlation to DBFM values, with a small bias in the PMROx$_{ASL}$ measurements.

LOWER METABOLIC CONDITION

A significant reduction in WB CBF was observed between the two metabolic conditions for OxFlow and pCASL: 33.4 ± 14.8 and 39.0 ± 19.6 mL/100g/min, respectively (Fig. 3 and 5A). There was a corresponding significant increase in OEF of 0.11 ± 0.06 (Fig. 5B) measured by OxFlow, and a significant reduction in WB-$CMRO_2$ measured by PMROx and PMROx$_{ASL}$: 0.68 ± 0.36 and 0.67 ± 0.36 mLO_2/100g/min, respectively; (Fig. 3 and 5C).

DISCUSSION

[^{15}O]O_2-PET has been used extensively to assess disruptions in cerebral energy metabolism, such as following stroke, predicting its risk of recurrence, and understanding energy regulation during functional activation (*21*). Despite the proven value of [^{15}O]O_2-PET, the procedure is complex and invasive, which has led to a diminishing number of sites with the necessary expertise to conduct [^{15}O]O_2 studies. This trend highlights the value to develop simpler [^{15}O]O_2 imaging protocols that retain the inherent quantitative capabilities of PET. This study focused on validating a hybrid PET/MR technique developed specifically to address this issue. The possibility of using PET/MR to update [^{15}O]O_2 imaging was investigated by Su *et al*., who used MRI to extract image-derived AIFs (*9*). The current study explored an alternative approach using WB MRI measurements as a reference, which avoids potential registration and partial volume errors. PMROx is also less sensitive to errors caused by RW and the CBV since regional $CMRO_2$ is determined from the ratio of TACs. The validity of this approach was demonstrated in a recent paper expanding Eq. (7) to include RW and CBV (*20*).

Validation experiments were conducted using a porcine animal model and involved imaging $CMRO_2$ independently using the previously validated DBFM (*6*). For this method, an MR-compatible arterial sampling system was used to measure the AIF for both tracers. Good agreement between PMROx and DBFM was found across ROIs with respect to both OEF and $CMRO_2$, although a small bias was observed in the PMROx $CMRO_2$ estimates (Fig. 2F). Regression analysis also demonstrated strong and moderate correlations between techniques for OEF and $CMRO_2$, respectively. The lower correlation for the latter is explained by its dependency on both OEF and CBF. In addition to the agreement with DBFM, PMROx was shown to be sensitive to reduced energy metabolism caused by increasing the propofol infusion. The $CMRO_2$

reduction was driven by the propofol-induced decrease in CBF, since propofol caused an increase in OEF. These findings are in agreement with Oshima *et al.* who reported that propofol caused proportional decreases in CBF and $CMRO_2$, but had no effect on the arteriovenous oxygen difference (*22*).

Since the PMROx approach scales the $[^{15}O]O_2$ images by an MRI estimate of WB $CMRO_2$, its accuracy and precision will be directly affected by the MRI methods used to calculate WB OEF and CBF. In this study, WB OEF and $CMRO_2$ were measured by OxFlow, which can be acquired with scan times as short as 8 s with reproducibility of 2% for S_vO_2 and 6% for WB $CMRO_2$ (*23*). The current study presents the first simultaneous comparison of OxFlow to $[^{15}O]H_2O$ and $[^{15}O]O_2$ PET with no significant differences found between techniques. This agreement is in accordance with two recent studies comparing MR measurements of S_vO_2 to either PET or direct measures from the jugular blub (*24*,*25*).

PET/MR also provides the possibility of reduces the PET procedure to $[^{15}O]O_2$ inhalation only by replacing $[^{15}O]H_2O$ PET with ASL ($PMROx_{ASL}$). WB CBF estimates from pCASL were in good agreement to those obtained by $[^{15}O]H_2O$ PET, similar to previous ASL/PET comparisons conducted using a swine model (*10*,*26*). Strong correlations between regional CBF measurements were found for all ROIs except the cerebellum, which was attributed to limited spatial coverage for the pCASL sequence. Recent studies comparing ASL to PET involving human participants suggest that ASL can provide accurate CBF measurements with careful attention to common sources of error (*27*). Its translation to clinical studies remains an active area of research as factors such as cerebrovascular disease and ageing can impact its accuracy and precision (*28*).

A challenge with PET-only imaging is correcting for signal contamination from the CBV (*4*). Blood volume terms were incorporated into the fitting procedure for both tracers. Although

the average V_b^w was larger than reported in human studies, it is in accordance with Olsen *et al*. who reported values from 9 to 18 mL/100g in pigs, depending on P_aCO_2 (*29*). The V_0^o values were smaller since they are scaled by OEF and the venous fraction. WB V_A^w estimates were very small for most animals, as expected, as it only becomes significant in highly vascularized regions (*6*). In one animal, V_A^w reached a non-physiological value of 19.1 mL/100g, which was likely a result of estimating $A_w(t)$ using a physiologic model.

CONCLUSION

In summary, this study presents the validation of a non-invasive hybrid PET/MR technique, PMROx, to image $CMRO_2$ that only requires a short inhalation of $[^{15}O]O_2$, followed by 5 min of PET and simultaneous MR imaging. Good agreement between $CMRO_2$ values from PMROx and the DBFM was found, and the proposed method was shown to be sensitive to reduced cerebral metabolism induced by increasing the anaesthetic level.

DISCLOSURE

This work was supported by the Canadian Institutes of Health Research, grant 148600. There is no potential conflict of interest relevant to this article.

KEY POINTS

QUESTION: Can MRI measurements be used to calibrate $[^{15}O]O_2$-PET data to determine the cerebral metabolic rate of oxygen ($CMRO_2$) in a PET/MR scanner?

PERTINENT FINDINGS: The proposed PMROx approach resulted in similar $CMRO_2$ measurements when compared to those from a PET-only technique. PMROx was further simplified by incorporating ASL, and it proved sensitive to anaesthetics-induced changes in metabolism.

IMPLICATIONS FOR PATIENT CARE: PMROx is a non-invasive technique that requires only $[^{15}O]O_2$, which facilitates its application in humans studies, and it may prove to be a useful tool to better understand disorders characterized by disruptions in cerebral oxidative metabolism.

REFERENCES

1. Lin W, Powers WJ. Oxygen metabolism in acute ischemic stroke. *J Cereb Blood Flow Metab*. 2018;38:1481-1499.

2. Vaishnavi SN, Vlassenko AG, Rundle MM, Snyder AZ, Mintun MA, Raichle ME. Regional aerobic glycolysis in the human brain. *Proc Natl Acad Sci U S A*. 2010;107:17757-62.

3. Baron JC, Jones T. Oxygen metabolism, oxygen extraction and positron emission tomography: Historical perspective and impact on basic and clinical neuroscience. *Neuroimage*. 2012;61:492-504.

4. Mintun MA, Raichle ME, Martin WR, Herscovitch P. Brain oxygen utilization measured with O-15 radiotracers and positron emission tomography. *J Nucl Med*. 1984;25:177-87.

5. Kudomi N, Hayashi T, Teramoto N, et al. Rapid quantitative measurement of CMRO2 and CBF by dual administration of 15O-labeled oxygen and water during a single PET scan - A validation study and error analysis in anesthetized monkeys. *J Cereb Blood Flow Metab*. 2005;25:1209-1224.

6. Kudomi N, Hirano Y, Koshino K, et al. Rapid quantitative CBF and CMRO2 measurements from a single PET scan with sequential administration of dual 15O-labeled tracers. *J Cereb Blood Flow Metab*. 2013;33:440-448.

7. Ohta S, Meyer E, Thompson CJ, Gjedde A. Oxygen consumption of the living human brain measured after a single inhalation of positron emitting oxygen. *J Cereb Blood Flow Metab*. 1992;12:179-192.

8. Kudomi N, Maeda Y, Yamamoto H, Yamamoto Y, Hatakeyama T, Nishiyama Y. Reconstruction of input functions from a dynamic PET image with sequential

administration of 15O2 and H215O for noninvasive and ultra-rapid measurement of CBF, OEF, and CMRO2. *J Cereb Blood Flow Metab*. 2018;38:780-792.

9. Su Y, Vlassenko AG, Couture LE, et al. Quantitative hemodynamic PET imaging using image-derived arterial input function and a PET/MR hybrid scanner. *J Cereb Blood Flow Metab*. 2017;37:1435-1446.

10. Ssali T, Anazodo UC, Thiessen JD, Prato FS, St. Lawrence K. A noninvasive method for quantifying cerebral blood flow by hybrid PET/MRI. *J Nucl Med*. 2018;59:1329-1334.

11. Alsop DC, Detre JA, Golay X, et al. Recommended implementation of arterial spin-labeled Perfusion mri for clinical applications: A consensus of the ISMRM Perfusion Study group and the European consortium for ASL in dementia. *Magn Reson Med*. 2015;73:102-116.

12. Wehrli FW, Rodgers ZB, Jain V, et al. Time-resolved MRI oximetry for quantifying CMRO2 and vascular reactivity. *Acad Radiol*. 2014;21:207-214.

13. Jain V, Langham MC, Wehrli FW. MRI estimation of global brain oxygen consumption rate. *J Cereb Blood Flow Metab*. 2010;30:1598-1607.

14. Cockburn N, Corsaut J, Kovacs MS, St. Lawrence K, Hicks JW. Validation protocol for current good manufacturing practices production of [15O]water for hybrid PET/MR studies. *Nucl Med Commun*. July 2020.

15. Iguchi S, Moriguchi T, Yamazaki M, et al. System evaluation of automated production and inhalation of 15O-labeled gaseous radiopharmaceuticals for the rapid 15O-oxygen PET examinations. *EJNMMI Phys*. 2018;5:1-21.

16. Hori Y, Hirano Y, Koshino K, et al. Validity of using a 3-dimensional PET scanner during inhalation of 15 O-labeled oxygen for quantitative assessment of regional metabolic rate of

oxygen in man. *Phys Med Biol*. 2014;59:5593-5609.

17. Carney JPJ, Townsend DW, Rappoport V, Bendriem B. Method for transforming CT images for attenuation correction in PET/CT imaging. *Med Phys*. 2006;33:976-983.

18. Kudomi N, Hayashi T, Watabe H, et al. A physiologic model for recirculation water correction in CMRO2 assessment with 15O2 inhalation PET. *J Cereb Blood Flow Metab*. 2009;29:355-364.

19. Severinghaus JW. Simple, accurate equations for human blood O2 dissociation computations. *J Appl Physiol Respir Environ Exerc Physiol*. 1979.

20. Narciso L, Ssali T, Iida H, St. Lawrence K. A non-invasive reference-based method for imaging the cerebral metabolic rate of oxygen by PET/MR: Theory and error analysis. Manuscript submitted for publication. *Phys Med Biol*. 2020.

21. Vafaee MS, Vang K, Bergersen LH, Gjedde A. Oxygen consumption and blood flow coupling in human motor cortex during intense finger tapping: Implication for a role of lactate. *J Cereb Blood Flow Metab*. 2012;32:1859-1868.

22. Oshima T, Karasawa F, Satoh T. Effects of propofol on cerebral blood flow and the metabolic rate of oxygen in humans. *Acta Anaesthesiol Scand*. 2002;46:831-835.

23. Barhoum S, Langham MC, Magland JF, et al. Method for rapid MRI quantification of global cerebral metabolic rate of oxygen. *J Cereb Blood Flow Metab*. 2015;35:1616-1622.

24. Miao X, Nayak KS, Wood JC. In vivo validation of T2- and susceptibility-based SvO2 measurements with jugular vein catheterization under hypoxia and hypercapnia. *Magn Reson Med*. 2019;82:2188-2198.

25. Jiang D, Deng S, Franklin CG, et al. Validation of T2-based oxygen extraction fraction

measurement with 15O positron emission tomography. *Magn Reson Med*. July 2020:mrm.28410.

26. Andersen JB, Henning WS, Lindberg U, et al. Positron emission tomography/magnetic resonance hybrid scanner imaging of cerebral blood flow using 15O-water positron emission tomography and arterial spin labeling magnetic resonance imaging in newborn piglets. *J Cereb Blood Flow Metab*. 2015;35:1703-1710.

27. Puig O, Henriksen OM, Vestergaard MB, et al. Comparison of simultaneous arterial spin labeling MRI and 15O-H2O PET measurements of regional cerebral blood flow in rest and altered perfusion states. *J Cereb Blood Flow Metab*. 2020;40:1621-1633.

28. Fan AP, Jahanian H, Holdsworth SJ, Zaharchuk G. Comparison of cerebral blood flow measurement with [15O]-water positron emission tomography and arterial spin labeling magnetic resonance imaging: A systematic review. *J Cereb Blood Flow Metab*. 2015;36:842-861.

29. Olsen AK, Keiding S, Munk OL. Effect of hypercapnia on cerebral blood flow and blood volume in pigs studied by positron emission tomography. *Comp Med*. 2006;56:416-420.

FIGURE LEGENDS

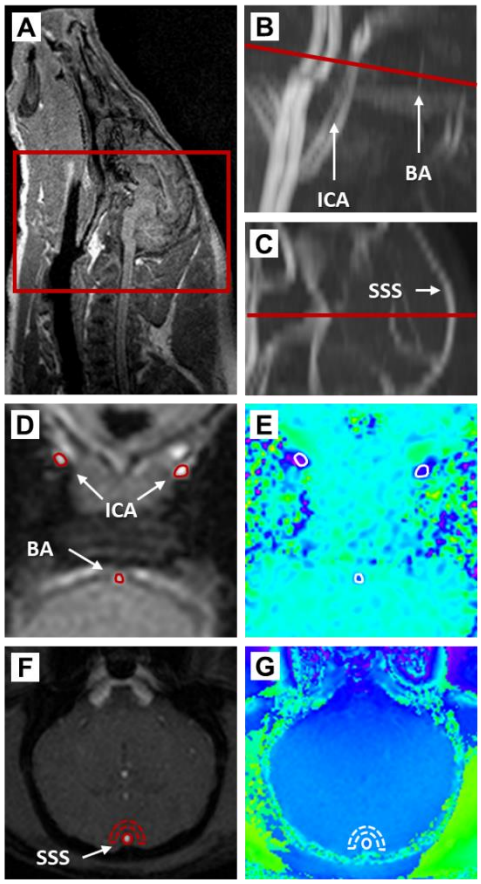

FIGURE 1. (A) Sagittal MPRAGE image showing imaging region. MR angiography showing (B) the internal carotid arteries (ICA) and basilar artery (BA), and (C) the superior sagittal sinus (SSS). The red lines represent the slices used to measure WB CBF and SvO_2. Magnitude images from the slices used to estimate (D) WB CBF and (F) S_vO_2, and their respective phase components (E) and (G). The red ROIs were transferred from the magnitude to the phase image (in white). All images are from one representative animal.

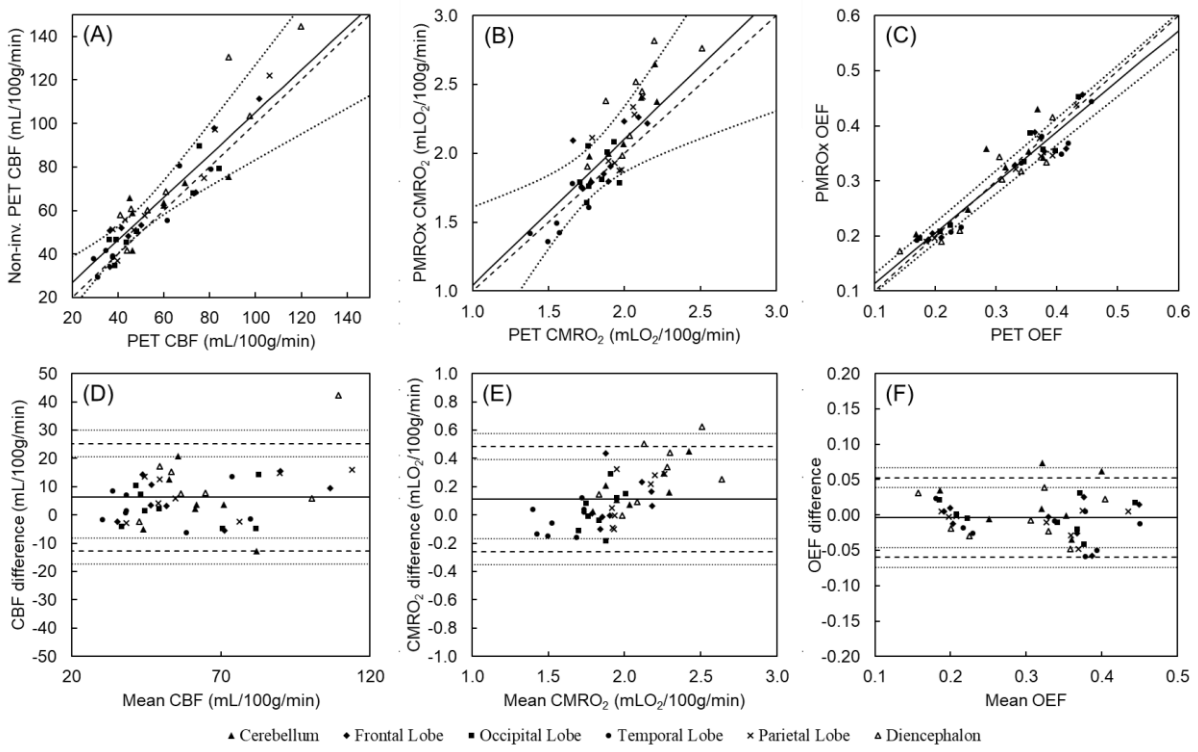

FIGURE 2. (A) Local baseline CBF from non-invasive PET/MR and DBFM. Average regression line is represented by the solid line ($y = 0.98x + 7.29$; 95% confidence interval (CI) is represented by the dotted lines). The dashed line is the identity line. Corresponding (B) OEF and (C) $CMRO_2$ results presented average regression line of $y = 0.92x + 0.02$ and $y = 1.06x - 0.02$, respectively. Bland-Altman plots from the corresponding data are presented in (D)-(F), where the mean is represented by the solid line. The dashed lines represent the limits of agreement (±2 SDs), each with its 95% CI (dotted lines). Mean difference from the Bland-Altman analysis was 6.2 mL/100g/min for CBF ($p < 0.01$), -0.004 (ns) for OEF and 0.11 mLO_2/100g/min ($p < 0.01$) for $CMRO_2$.

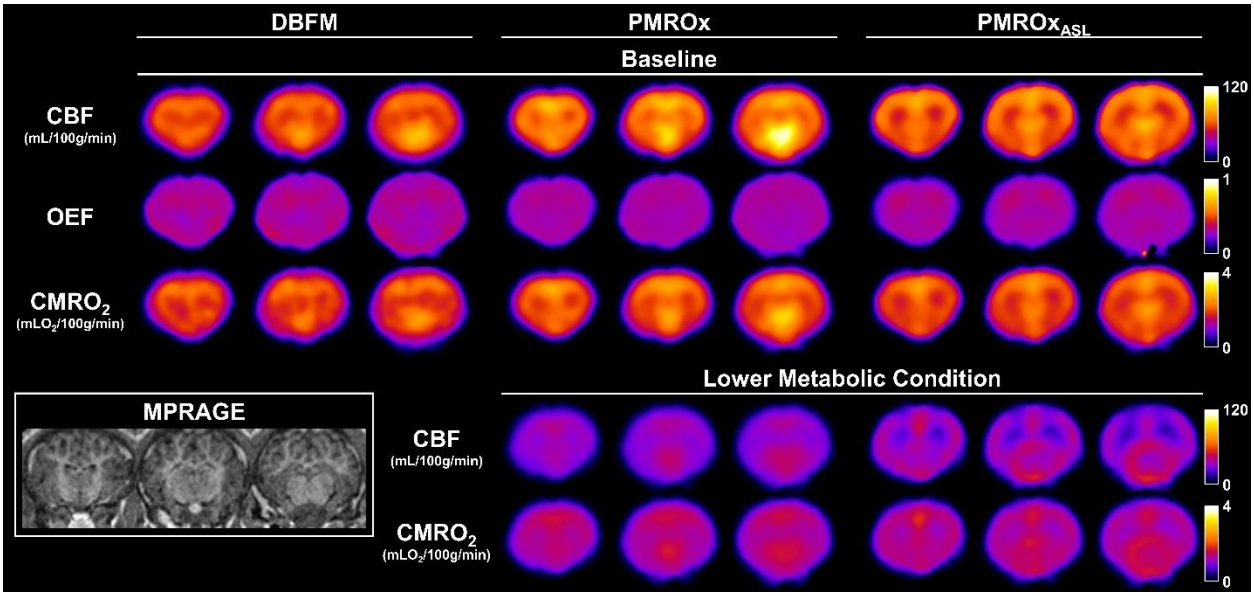

FIGURE 3. Group-wise CBF, OEF and $CMRO_2$ images obtained with DBFM, PMROx and $PMROx_{ASL}$ techniques for baseline (n = 8, top three rows). CBF and $CMRO_2$ results from PMROx and $PMROx_{ASL}$ for the lower metabolic condition (n = 6) are presented on the bottom two rows. MPRAGE from one animal was included for anatomical reference.

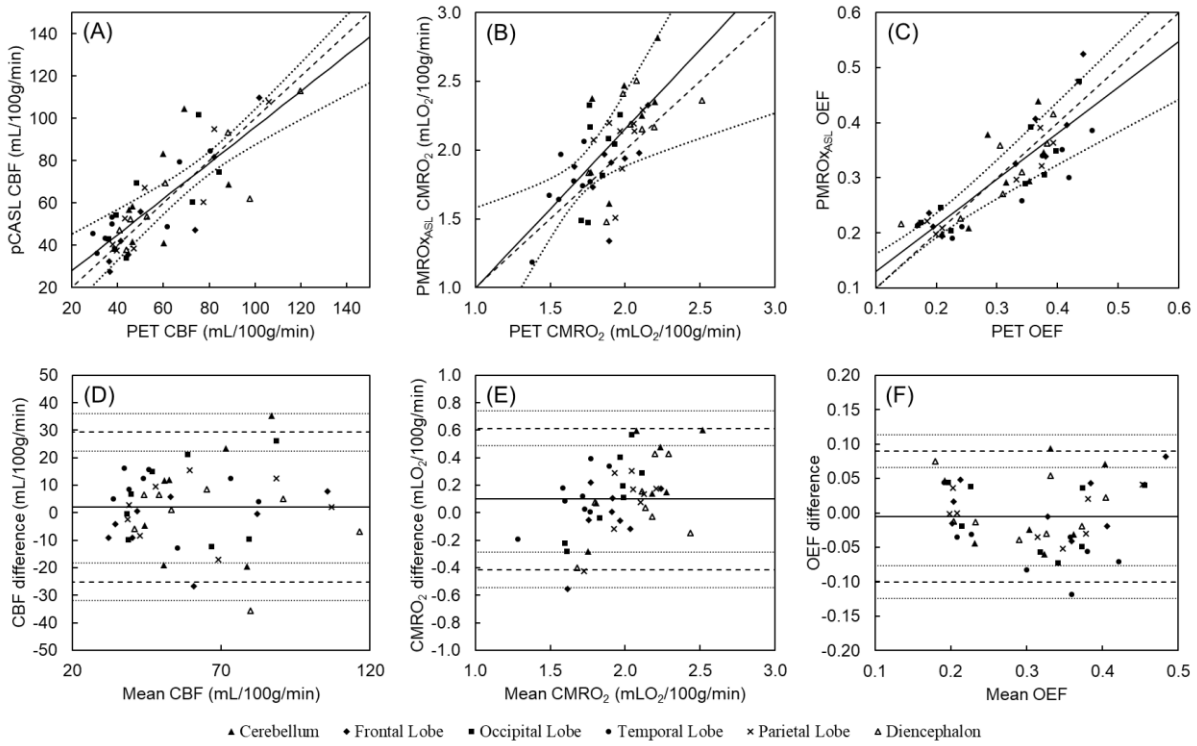

FIGURE 4. (A) Local baseline CBF from pCASL and DBFM. Average regression line is represented by the solid line ($y = 0.85x + 10.91$; 95% confidence interval (CI) is represented by the dotted lines). The dashed line is the identity line. Corresponding (B) OEF and (C) $CMRO_2$ results presented average regression line of $y = 0.83x + 0.05$ and $y = 1.15x - 0.16$, respectively. Bland-Altman plots from the corresponding data are presented in (D)-(F), where the mean is represented by the solid line. The dashed lines represent the limits of agreement (±2 SDs), each with its 95% CI (dotted lines). Mean difference from the Bland-Altman analysis was 2.1 mL/100g/min for CBF (ns.), -0.005 (ns) for OEF and 0.10 mLO_2/100g/min (p = 0.01) for $CMRO_2$.

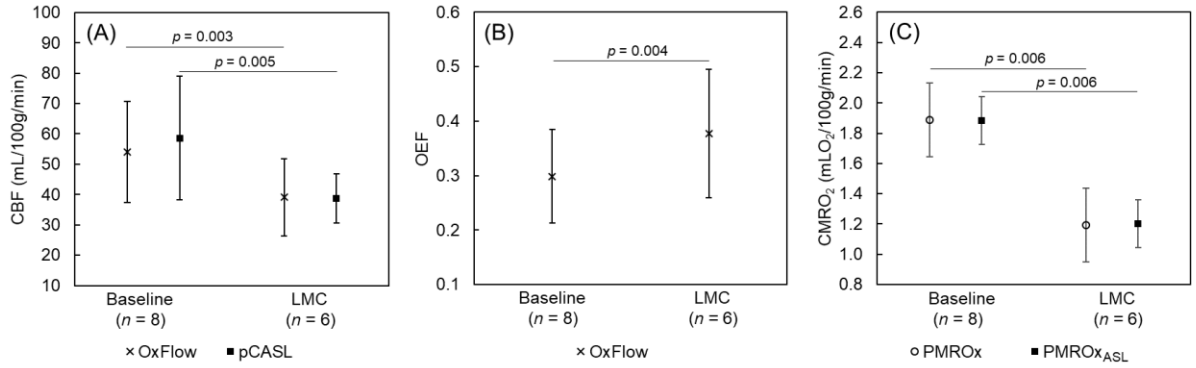

FIGURE 5. (A) WB CBF, (B) OEF and (C) $CMRO_2$ values for baseline and LMC. Significant reductions in WB-CBF and WB-$CMRO_2$ were observed for both techniques, while a significant increase was observed for WB-OEF.

TABLES

TABLE 1. Summary of arterial blood measurements. No statistical differences were identified in any of the parameters across the acquisitions.

	Baseline	**LMC**
Hematocrit (%)	25.9 ± 3.4	25.7 ± 2.1
Hemoglobin (g/dL)	8.3 ± 1.1	8.3 ± 0.7
P_aO_2 (mmHg)	230 ± 100	239 ± 102
P_aCO_2 (mmHg)	40.3 ± 4.3	41.0 ± 3.4
S_aO_2 (%)	99.5 ± 0.5	99.5 ± 0.4
Glucose concentration (mmol/L)	5.5 ± 0.8	5.5 ± 0.4

TABLE 2. Summary of the regression and correlation analyses performed on the local measurements of CBF (mL/100g/min), OEF and $CMRO_2$ (mLO_2/100g/min).

		Slope	**Intercept**	***R^2***	***ρ***
PMROx	CBF	0.98 ± 0.20	7.3 ± 9.8	0.86 ± 0.10	0.91 ± 0.10
	OEF	0.92 ± 0.03*	0.02 ± 0.01†	0.91 ± 0.06	0.95 ± 0.04
	$CMRO_2$	1.06 ± 0.35	-0.02 ± 0.63	0.49 ± 0.26	0.67 ± 0.20
$PMROx_{ASL}$	CBF	0.85 ± 0.15	10.9 ± 11.7	0.66 ± 0.24	0.80 ± 0.18
	OEF	0.83 ± 0.13*	0.05 ± 0.03†	0.77 ± 0.14	0.87 ± 0.09
	$CMRO_2$	1.15 ± 0.41	-0.16 ± 0.70	0.30 ± 0.15	0.53 ± 0.14

*Significantly different than one.

†Significantly different than zero.